

Near-Unitary Spin Squeezing in ^{171}Yb

Boris Braverman,^{1,* ‡} Akio Kawasaki,^{1,† ‡} Edwin Pedrozo-Peñafiel,^{1,‡} Simone Colombo,¹ Chi Shu,^{1,2} Zeyang Li,¹ Enrique Mendez,¹ Megan Yamoah,¹ Leonardo Salvi,^{1,3} Daisuke Akamatsu,^{1,4} Yanhong Xiao,^{1,5} and Vladan Vuletić^{1, §}

¹*Department of Physics, MIT-Harvard Center for Ultracold Atoms and Research Laboratory of Electronics, Massachusetts Institute of Technology, Cambridge, Massachusetts 02139, USA*

²*Department of Physics, Harvard University, Cambridge, Massachusetts 02138, USA*

³*Dipartimento di Fisica e Astronomia and LENS - Università di Firenze, INFN - Sezione di Firenze, Via Sansone 1, 50019 Sesto Fiorentino, Italy*

⁴*National Metrology Institute of Japan (NMIJ), National Institute of Advanced Industrial Science and Technology (AIST), 1-1-1 Umezono, Tsukuba, Ibaraki 305-8563, Japan*

⁵*Department of Physics, State Key Laboratory of Surface Physics and Key Laboratory of Micro and Nano Photonic Structures (Ministry of Education), Fudan University, Shanghai 200433, China*

(Dated: March 10, 2022)

We report nearly unitary spin squeezing between the magnetic sublevels of the ground state of ^{171}Yb , an atom with an optical clock transition. The collective spin of $\sim 10^3$ atoms inside a cavity is squeezed using light detuned from the system's resonances. We demonstrate an interferometer operating with a squeezed state of nearly Heisenberg-uncertainty-limited area that improves the averaging time over the standard quantum limit (SQL) by a factor of 3.7(2). The observed metrological gain is limited by the state readout to 9.4(4) dB, while the generated states offer a spin noise suppression of 15.8(3) dB and a metrological gain of 12.9(1) dB over the SQL. In the future, the demonstrated squeezing between nuclear spin states can be directly mapped onto an electronic optical-clock transition to improve the performance of an ^{171}Yb optical clock.

PACS numbers: 03.65.Aa, 03.67.Bg, 32.80.Qk

The precision of atomic sensors using ensembles of independent particles is bounded by the standard quantum limit (SQL): due to spin projection noise, a sensor operating with N uncorrelated atoms will have a precision \sqrt{N} times better than with a single atom. Spin squeezed states (SSSs) [1–21] are many-body entangled states that can provide precision beyond the SQL [3, 22]. Metrological applications require controlled interactions between the particles to prepare the SSS, that are then turned off during the actual measurement sequence. Optical techniques provide an effective switchable atom-atom interaction [7–12] that can be enhanced by a cavity [13–18].

Two optical methods have been used to generate SSSs in atomic ensembles. One is a quantum non-demolition (QND) measurement of the collective atomic spin using light [8–10, 14–18, 23, 24], yielding record levels of up to 20.1(3) dB of squeezing [16, 17]. The other is a quantum feedback mechanism where the atoms collectively influence the probe light inside the cavity, which then acts back onto the atoms (cavity feedback squeezing [13, 18, 25]). In experiments so far, both methods have produced mixed atomic states where the uncertainty area far exceeds that of the original unentangled coherent spin state (CSS). In both cases, the non-unitary evolution is caused by decoherence due to the loss of information about the system, that is in principle available, to an uncontrolled environment. The QND method is limited in practice by light losses and non-ideal measurement [24], while in standard cavity squeezing [13, 14] the emerging light carries unused information about the atomic state.

Recently, Zhang *et al.* [26] pointed out that in cavity squeezing, the non-unitary evolution can be minimized by detuning the probe light from cavity resonance. Although this decreases the squeezing strength per photon, it hides the information about the atomic state in the photon shot noise, improving the squeezing performance, and enabling near-unitary squeezing.

Here, motivated by future applications to optical-transition clocks [27–30], we demonstrate near-unitary optical spin squeezing using an adaptation of the scheme of Ref. [26]. Under conditions where the state area increases by less than 40%, we demonstrate a factor of 4 reduction in measurement time for a given precision compared to the SQL. The observed usable metrological gain of up to 9.4(4) dB is limited by the state detection, while subtraction of the independently determined measurement noise implies that the generated SSSs offer 12.9(1) dB of metrological gain and 15.8(3) dB of spin noise suppression. The squeezing is achieved between the nuclear magnetic sublevels of the electronic ground state of ^{171}Yb [7] and can be mapped in the future directly onto the optical-clock transition [31].

Cold ^{171}Yb atoms are prepared in a two-color magneto-optical trap (MOT) [32] and then cooled further in a single-color MOT on the triplet transition $^1S_0 \rightarrow ^3P_1$ with wavelength $\lambda=556$ nm and linewidth $\Gamma/(2\pi)=184$ kHz. The atoms are transported into an asymmetric high-finesse optical cavity [33] by adjusting the bias magnetic field, where they are loaded into a one-dimensional optical lattice with wavelength $\lambda_t=759$ nm, corresponding to

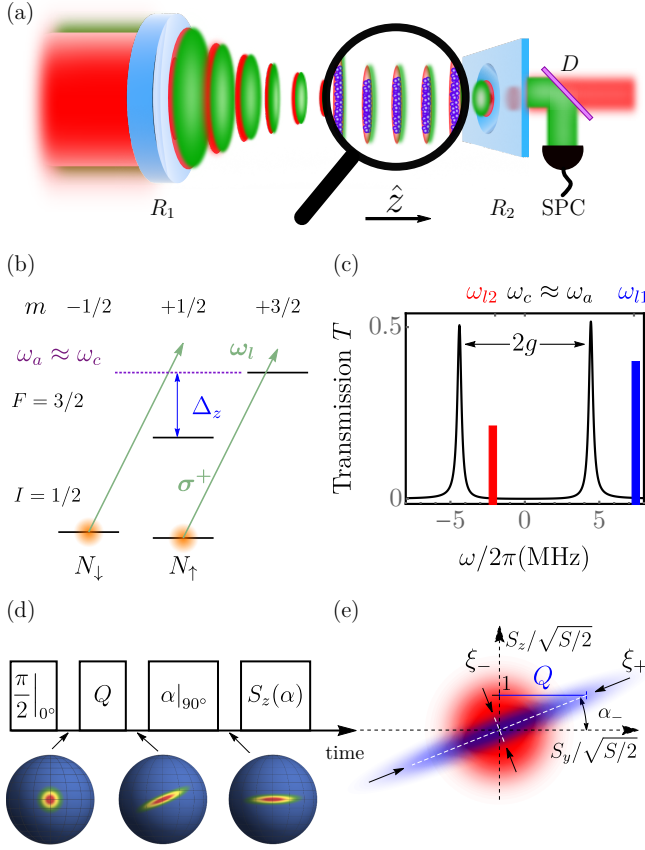


FIG. 1. (a) Schematic diagram of the asymmetric cavity and atoms used in the experiment. $\lambda_t=759$ nm light (red beam) is used to create the 1-D optical lattice to trap the atoms, and $\lambda=556$ nm light (green beam) is used as squeezing and probing light, whose transmission is detected using a single photon counter (SPC) after being separated from the transmitted trap light at the dichroic mirror (D). The two cavity mirrors have curvatures of $R_1=25$ mm and $R_2\approx 350$ μm , respectively. (b) Relevant energy levels of ^{171}Yb . The lower two are for the 1S_0 ground state with nuclear spin $I=1/2$, and the higher two are in $^3P_1, F=3/2$ manifold. The energy levels account for Zeeman splitting with $\Delta_z=2\pi\times 18.5$ MHz. (c) Cavity transmission spectrum showing vacuum Rabi splitting for $N\eta=1800$ and the frequencies of the two squeezing light pulses ω_{l1} and ω_{l2} . (d) Simplified experimental sequence for generating and measuring the spin squeezing. (e) A cartoon of the distributions on Bloch sphere near the x axis for a coherent state (red) and squeezed state (blue).

the magic trapping wavelength for the $^1S_0\rightarrow^3P_0$ optical-clock transition [34] for future applications. Over 85 ms, the trap depth U_0 is lowered from $U_0=k_B\times 120$ μK to $U_0/3$ and restored to U_0 in order to remove hot atoms with weaker coupling to the cavity mode. The temperature of the remaining $N_{\text{tot}}\approx 1500$ atoms is $T=(20\pm 5)$ μK .

The asymmetric cavity consists of a large spherical mirror with radius of curvature $R_1=25$ mm, and a slightly elliptical micromirror with $R_2=303\times 391$ μm [33]. The cavity finesse is $\mathcal{F}=1.3\times 10^4$ for light at wavelength

$\lambda=2\pi/k=556$ nm, corresponding to a cavity linewidth $\kappa/(2\pi)=480$ kHz. The single-atom cooperativity parameter at an antinode is given by $\eta_0=24\mathcal{F}/(\pi k^2 w^2)$ [35]. At a distance of 0.42 mm from the micromirror, the mode waist ($1/e^2$ intensity radius) equals $w=15.1$ μm , giving $\eta_0=2.4$, which means that the system is in the strong-coupling regime [36–38] (see also [33] for details). Atoms are inhomogeneously coupled to the probe field whose wavelength differs from the trapping light. As in Refs. [14, 39], we define an effective atom number $N=N_{\text{tot}}\langle\eta^2\rangle/\langle\eta\rangle^2=\frac{2}{3}N_{\text{tot}}$ and effective single-atom cooperativity $\eta=\langle\eta^2\rangle/\langle\eta\rangle=\frac{3}{4}\eta_0$, so that the spin projection noise, measured via the cavity, satisfies the usual relation $(\Delta N)^2=N/4$ for a CSS. The experiments described below are performed with $N\approx 1000$, $\eta=1.8(1)$, and a collective cooperativity $N\eta\approx 1800$. The effective cooperativity η is confirmed in an independent measurement (see Supplemental Material (SM) [40]).

We perform squeezing between the nuclear sublevels $|\uparrow\rangle\equiv|m_I=\frac{1}{2}\rangle$ and $|\downarrow\rangle\equiv|m_I=-\frac{1}{2}\rangle$ of the electronic 1S_0 ground state of ^{171}Yb . The collective spin state can be represented on a Bloch sphere with radius $S=N/2$ [39]. The cavity frequency ω_c is tuned to be nearly resonant ($\omega_c-\omega_a=2\pi\times -340$ kHz) with the $|\uparrow\rangle\rightarrow|{}^3P_1, m_F=\frac{3}{2}\rangle$ atomic transition with frequency ω_a in the presence of a magnetic field $B_z=13.6$ G along the cavity axis. N_\uparrow atoms in the state $|\uparrow\rangle$ induce a vacuum Rabi splitting $2g=\sqrt{N_\uparrow\eta\kappa\Gamma}$ of the cavity resonance. Near the equator of the Bloch sphere, where $N_\downarrow\approx N_\uparrow$, there is also a small dispersive effect from the N_\downarrow atoms in the state $|\downarrow\rangle$, suppressed by the Zeeman splitting $\Delta_z=2\pi\times 18.5$ MHz between magnetic sublevels in the excited 3P_1 state, with $\Delta_z\gg\Gamma, \kappa$, see Fig. 1 (b). To accurately analyze the experiments described below, we need to consider both the near-resonant transition $|\uparrow\rangle\rightarrow|{}^3P_1, m_F=\frac{3}{2}\rangle$ and the detuned transition $|\downarrow\rangle\rightarrow|{}^3P_1, m_F=\frac{1}{2}\rangle$.

S_z is determined by detecting N_\uparrow via a measurement of the Rabi splitting $2g$, swapping the populations of $|\uparrow\rangle$ and $|\downarrow\rangle$ with a radiofrequency π pulse, and remeasuring the Rabi splitting to give N_\downarrow . From N_\uparrow and N_\downarrow , we determine $S_z=(N_\uparrow-N_\downarrow)/2$, and $S=(N_\uparrow+N_\downarrow)/2$ using the two-transition atomic model and the separately measured cavity parameters (see SM [40]). The primary quantity of interest, denoted by $\sigma^2\equiv 2(\Delta S_z)^2/S$, is the spin variance $(\Delta S_z)^2$ normalized to the noise $(\Delta S_z)_{\text{CSS}}^2=S/2$ of the CSS.

The measured spin variance σ^2 is the sum of the variances of the atomic state σ_{st}^2 and the measurement resolution σ_d^2 . To quantify the latter, we prepare a CSS on the equator, measure S_z twice, and divide the variance of the measurement difference $S_{z1}-S_{z2}$ by 2. We achieve a detection variance $\sigma_d^2=-9.4(4)$ dB, i.e. a factor of 9 below the SQL, for the collective cooperativity $N\eta=1800$ at which we operate. As in previous implementations of optical spin squeezing [16, 17, 25], the measurement quality

is limited by the finite photon detection efficiency of 15% and by Raman scattering that randomly transfers atoms between the states $|\uparrow\rangle$ and $|\downarrow\rangle$ [24, 41], (see SM [40]).

The spin squeezing sequence is shown in Fig. 1 (d). First, we create a CSS along the x -axis by optically pumping all atoms into $|\uparrow\rangle$, and then applying a $\pi/2$ -pulse. The squeezing is generated by pulses of light with frequency ω_l detuned from the vacuum Rabi peaks. The value of ω_l is based on a compromise between two effects of larger detuning from the Rabi peaks: more unitary squeezing, and more contrast loss (shrinking of the Bloch sphere) due to less squeezing per photon, and hence more photon scattering into free space. We send two σ^+ -polarized laser pulses through the atom-cavity system, with detunings $\omega_{l1}-\omega_a=2\pi\times 7.33$ MHz and $\omega_{l2}-\omega_a=-2\pi\times 2$ MHz, and a relative incident power ratio $P_2/P_1=0.53$. Both pulses produce one-axis twisting [1] (cavity feedback squeezing [13]) of the collective atomic spin in the same direction, while their detunings and relative power are chosen in order to cancel, to first order, the dependence of the twisting strength on the total atom number near $N\approx 1000$.

Besides the squeezing, the intracavity light also shifts the phase of the CSS, which we cancel by a spin echo sequence (see SM [40]). Finally, in order to reconstruct the SSS and its minimum and maximum variances, we rotate the state by an angle α about its average spin vector and detect the spin projection along the z axis $S_z(\alpha)$ (see Fig. 1(d)).

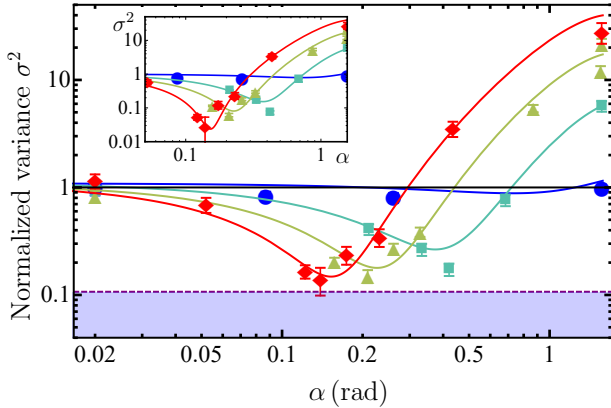


FIG. 2. Measured spin noise $\sigma^2(\alpha)$ (data points) normalized to the SQL, as a function of rotation angle α of the squeezed state, for shearing strengths $Q = 0.3$ (blue circles), $Q = 2.2$ (green squares), $Q = 4.5$ (yellow triangles), and $Q = 6.6$ (red diamonds). For visualization, the data measured at $\alpha=0$ are displayed at $\alpha=0.02$ rad. The solid lines are theoretical fits, the dashed line at $\sigma^2=0.11$ indicates the detection limit; states in the blue region below the line cannot be directly observed. Inset: σ_{st}^2 of SSS after subtracting measurement noise, indicating $14.5^{+0.8}_{-1.2}$ dB of spin noise suppression.

The collective spin state is reconstructed by measuring

$S_z(\alpha)$ for more than 100 identically prepared states for each state rotation angle α . The normalized spin variance $\sigma^2(\alpha)=2(\Delta S_z(\alpha))^2/S$ along the direction α is displayed in Fig. 2 for several different shearing strengths. As a given SSS is rotated, the projected variance dips below the CSS noise until the rotation angle α reaches α_- , where the short axis of the ellipse lies along the z -axis. Beyond α_- , the variance increases again, crosses the CSS noise again at $\alpha=2\alpha_-$, and grows until the antisqueezing quadrature is oriented along z for $\alpha\approx\pi/2$.

To compare the data to a theoretical model, we first consider the polar angle of the spin vector, defined as $\tau_\alpha\equiv\sqrt{2S}\arcsin(S_z(\alpha)/S)$. Its variance $(\Delta\tau_\alpha)^2$, normalized to the variance $(\Delta\theta)_{CSS}^2=(2S)^{-1}$ of the CSS, is given by

$$\frac{(\Delta\tau_\alpha)^2}{(\Delta\theta_{CSS})^2} = 1 - Q \sin 2\alpha + (F + Q^2) \sin^2 \alpha. \quad (1)$$

Here, Q is the dimensionless shearing strength (see Fig. 1 (e)), defined as the normalized light-induced phase shift $\pm\phi/\Delta\theta_{CSS}$ experienced by a spin displaced by one standard deviation of the CSS from the equator, $S_z = \pm\sqrt{S/2}$ [13]. The other dimensionless parameter F quantifies the excess broadening (in variance units) compared to a pure SSS or CSS, which have $F = 0$. (For an explicit expression for Q and F see SM [40].)

From (1) we find the minimum (ξ_-^2) and maximum (ξ_+^2) variances of the normalized spin angle τ_α ,

$$\xi_{\pm}^2 = \frac{1}{2} \left(2 + F + Q^2 \pm \sqrt{4Q^2 + (F + Q^2)^2} \right), \quad (2)$$

obtained at angles $\alpha_- = \arctan[(\sqrt{4Q^2 + (F + Q^2)^2} - (F + Q^2))/(2Q)]$ and $\alpha_+ = \alpha_- + \pi/2$, respectively. The normalized uncertainty area of the SSS ellipse is given by $A = \xi_+ \xi_- = \sqrt{1 + F}$. Since we do not measure angles but S_z projections, we need to take into account that the normalized spin variance $\sigma^2(\alpha)$ of $S_z(\alpha)$ is reduced relative to $(\Delta\tau_\alpha)^2$ by $\sigma^2(\alpha) = S/4[1 - \exp(-(\Delta\tau_\alpha)^2 4/S)]$. For the CSS and SSS quadrature ξ_-^2 , the approximation $\sigma^2(\alpha) \approx (\Delta\tau_\alpha)^2$ holds, while the observed antisqueezed quadrature ξ_+^2 is reduced by projection of the curved surface of the Bloch sphere onto the z axis.

The solid lines in Fig. 2 are obtained by fitting the data to $\sigma^2(\alpha) + \sigma_d^2$ with Q and F as the only fitting parameters, while σ_d^2 is the previously measured detection limit. We find good agreement between the model and the data, allowing us to extract both the shearing strength Q and the excess broadening F . In Fig. 3 we plot Q and F versus the number p_t of transmitted photons during the optical squeezing. For negligible technical noise we expect both Q and F to be proportional to p_t (see [42] and SM [40]). The solid lines in Fig. 3 represent the predicted linear behavior of Q and F obtained from an analytical model of the system without any free parameters [42]; the dotted line includes the effect of finite measurement

quality $\sigma_d^2 = -9.4(4)$ dB, that affects the measurement of the squeezed quadrature $\xi_-^2 < 1$, and hence F , but not Q . The model without any free parameters agrees remarkably well with the measured Q and F , indicating the absence of major technical limitations other than the finite state detection quality σ_d^2 .

The attainable metrological gain depends not only on the reduced spin noise ξ_-^2 , but also on the signal $\langle |\tilde{S}| \rangle$ [3] which determines the contrast C of an interferometric measurement. The dominant loss of contrast is due to the scattering of photons into free space during squeezing, which projects atoms into either of the states $|\uparrow\rangle$ or $|\downarrow\rangle$. The measured Ramsey contrast as a function of Q is shown in Fig. 4, together with the a-priori prediction $C = C_0 \exp\left(-(Q/\tilde{Q} + Q^2)/N\right)$ with $C_0 = 0.97$ as the only fitting parameter. Here, $\tilde{Q} = 0.0362(7)$ is the independently measured shearing strength per scattered photon. The term Q/\tilde{Q} describes photon scattering into free space, while the second, smaller term accounts for the SSS wrapping around the Bloch sphere.

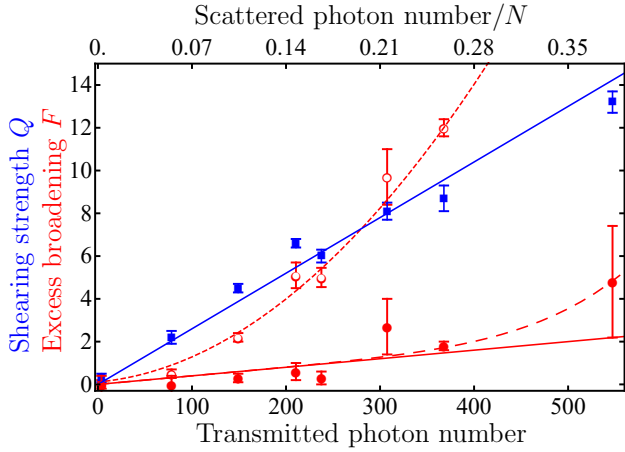


FIG. 3. Shearing strength Q (filled blue squares) and excess broadening factor F (red circles) extracted from the measured spin noise, plotted vs. the number of transmitted photons. The open red circles correspond to the directly measured data with theoretical model without free parameters (dotted red line), the solid circles are after subtraction of measurement noise σ_d^2 with parameter-free model without (solid red line) and with (dashed red line) Bloch sphere curvature induced-broadening.

The metrological gain of a squeezed state is then given by the Wineland parameter $\xi_W^2 = \xi_-^2 / C^2$ [3]. Fig. 4 (a) shows ξ_W^2 , the measured spin noise reduction ξ_-^2 , and the inferred squeezing $\xi_{st}^2 = \xi_-^2 - \sigma_d^2$ of the state after subtraction of the measurement resolution σ_d^2 . For $Q \gtrsim 6$ the measured squeezing ξ_-^2 saturates at σ_d^2 ; $Q = 6.5$ also optimizes the Wineland parameter at $\xi_W^2 = -6.5(1)$ dB. The inferred squeezing ξ_{st}^2 is consistent with the prediction from the model with no free parameters (solid red line), which is limited by the Bloch sphere curvature to

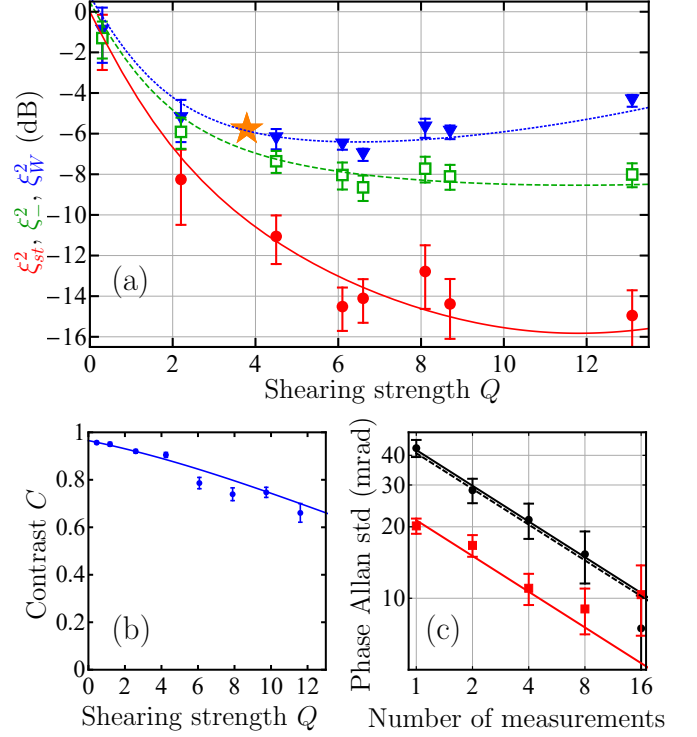


FIG. 4. (a) Wineland metrological gain ξ_W^2 (blue), measured spin noise reduction ξ_-^2 (green), and inferred spin noise of SSS ξ_{st}^2 (red) as a function of shearing strength Q . ξ_-^2 is limited by the measurement resolution and ξ_{st}^2 by the curvature of the Bloch sphere. (b) Contrast as a function of Q (data) with initial contrast as only fitting parameter (solid line). (c) Allan deviation of a phase measurement for a CSS (black squares) with SQL (dashed line) and for a SSS with $Q = 3.8$, $F = 0.8$ (red data). The red solid line is fit to first three red data points. The reduction in measurement time over SQL is a factor of 3.7(2), corresponding to $-5.8(3)$ dB. This result is represented by the orange star in (a).

$\xi_{st}^2 = -15.8(3)$ dB. The inferred metrological gain without readout noise is $\xi_W^2 = -12.9(1)$ dB.

Finally, we directly demonstrate an interferometric measurement with a precision beyond the SQL by implementing a Ramsey sequence with a squeezed, nearly uncertainty-limited input state (area $A = \sqrt{1+F} = 1.3$). We rotate the squeezed state by $\alpha = \pi/2 - \alpha_-$ to align the minimal uncertainty along the phase axis, allow the state evolve for a Ramsey time $\tau_R = 1.5$ ms, and apply a final $\pi/2$ rotation mapping the accumulated phase onto S_z . In Fig. 4(c), we compare the phase Allan deviation of the SSS (red squares) with that of the CSS (black circles). The precision of the CSS interferometer is accurately described by the SQL (black dashed line). For the given squeezing, with $Q = 3.8$, and $F = 0.8$, the SSS reaches the SQL precision with four times fewer measurements compared to a CSS interferometer. Larger squeezing yields better phase precision, but here it is our intent to demonstrate substantial improvement over the SQL

with a nearly uncertainty limited state $F \lesssim 1$ for clock applications [43].

In conclusion, we have demonstrated a method for generating near-unitary squeezed states via cavity feedback squeezing on a dilute ensemble of ^{171}Yb atoms. Our measurements agrees with a model without free parameters that predicts both the area and shape of the squeezed state. The results presented here can be further improved upon in several ways: state detection with a larger applied magnetic field will reduce the Raman scattering and improve the measured spin noise and metrological gain. The intrinsic squeezing of $\xi_{st}^2 = -16$ dB is already more than halfway (on a logarithmic scale) between the SQL and the ultimate Heisenberg limit at $\xi_H^2 = -30$ dB for $N=10^3$ atoms. The squeezing performance depends only on the collective cooperativity $N\eta$, and by placing the ensemble at a location in the cavity with higher single-atom cooperativity at constant $N\eta$, i.e. for smaller atom number, the demonstrated performance could already be quite close to the Heisenberg limit. Alternatively, by increasing the atom number at fixed η , the absolute squeezing should improve in proportion to $N\eta$. Near-unitary squeezing can be used for quantum information processing with Gaussian states [44, 45], and is useful for application to atomic clocks, where the antisqueezed component limits the Ramsey time [43]. We expect that the entanglement can be transferred from the nuclear spin directly to the ^{171}Yb clock transition through an optical π pulse, thus enabling optical-clock operation beyond the SQL in the near future.

We would like to thank Monika H. Schleier-Smith, James K. Thompson, and Mikhail Lukin for valuable discussions. This work was supported by NSF, DARPA, ONR, and the NSF Center for Ultracold Atoms (CUA). S. C. acknowledges support as a SNSF Early Postdoc Mobility fellow.

* bbraverm@uottawa.ca; Current address: Department of Physics and Max Planck Centre for Extreme and Quantum Photonics, University of Ottawa, 25 Templeton Street, Ottawa, Ontario K1N 6N5, Canada

† akiok@stanford.edu; Current address: W. W. Hansen Experimental Physics Laboratory and Department of Physics, Stanford University, Stanford, California 94305, USA

‡ These authors contributed equally

§ vuletic@mit.edu

- [1] M. Kitagawa and M. Ueda, *Phys. Rev. A* **47**, 5138 (1993).
- [2] D. J. Wineland, J. J. Bollinger, W. M. Itano, F. L. Moore, and D. J. Heinzen, *Phys. Rev. A* **46**, R6797 (1992).
- [3] D. J. Wineland, J. J. Bollinger, W. M. Itano, and D. J. Heinzen, *Phys. Rev. A* **50**, 67 (1994).
- [4] A. S. Sørensen and K. Mølmer, *Phys. Rev. Lett.* **86**, 4431 (2001).
- [5] A. Sørensen, L.-M. Duan, J. Cirac, and P. Zoller, *Nature* **409**, 63 (2001).
- [6] J. Ma, X. Wang, C.-P. Sun, and F. Nori, *Physics Reports* **509**, 89 (2011).
- [7] T. Takano, M. Fuyama, R. Namiki, and Y. Takahashi, *Phys. Rev. Lett.* **102**, 033601 (2009).
- [8] A. Kuzmich, L. Mandel, and N. P. Bigelow, *Phys. Rev. Lett.* **85**, 1594 (2000).
- [9] J. Appel, P. J. Windpassinger, D. Oblak, U. B. Hoff, N. Kjærgaard, and E. S. Polzik, *Proceedings of the National Academy of Sciences* **106**, 10960 (2009).
- [10] R. J. Sewell, M. Koschorreck, M. Napolitano, B. Dubost, N. Behbood, and M. W. Mitchell, *Phys. Rev. Lett.* **109**, 253605 (2012).
- [11] J. G. Bohnet, B. C. Sawyer, J. W. Britton, M. L. Wall, A. M. Rey, M. Foss-Feig, and J. J. Bollinger, *Science* **352**, 1297 (2016).
- [12] H. Bao, J. Duan, P. Li, X. Lu, W. Qu, M. Wang, I. Novikova, E. Mikhailov, K.-F. Zhao, H. Shen, and Y. Xiao, *arXiv:1811.06945* (2018).
- [13] I. D. Leroux, M. H. Schleier-Smith, and V. Vuletić, *Phys. Rev. Lett.* **104**, 073602 (2010).
- [14] M. H. Schleier-Smith, I. D. Leroux, and V. Vuletić, *Phys. Rev. Lett.* **104**, 073604 (2010).
- [15] J. G. Bohnet, K. C. Cox, M. A. Norcia, J. M. Weiner, Z. Chen, and J. K. Thompson, *Nature Photonics* **8**, 731 (2014).
- [16] K. C. Cox, G. P. Greve, J. M. Weiner, and J. K. Thompson, *Phys. Rev. Lett.* **116**, 093602 (2016).
- [17] O. Hosten, N. J. Engelsen, R. Krishnakumar, and M. A. Kasevich, *Nature* **529**, 505 (2016).
- [18] O. Hosten, R. Krishnakumar, N. J. Engelsen, and M. A. Kasevich, *Science* **352**, 1552 (2016).
- [19] C. D. Hamley, C. Gerving, T. Hoang, E. Bookjans, and M. S. Chapman, *Nature Physics* **8**, 305 (2012).
- [20] H. Kurkjian, K. Pawłowski, A. Sinatra, and P. Treutlein, *Phys. Rev. A* **88**, 043605 (2013).
- [21] M. F. Riedel, P. Böhi, Y. Li, T. W. Hänsch, A. Sinatra, and P. Treutlein, *Nature* **464**, 1170 (2012).
- [22] L. Pezzè, A. Smerzi, M. K. Oberthaler, R. Schmied, and P. Treutlein, *Reviews of Modern Physics* **90**, 035005 (2018).
- [23] A. Louchet-Chauvet, J. Appel, J. J. Renema, D. Oblak, N. Kjaergaard, and E. S. Polzik, *New Journal of Physics* **12**, 065032 (2010).
- [24] Z. Chen, J. G. Bohnet, J. M. Weiner, K. C. Cox, and J. K. Thompson, *Phys. Rev. A* **89**, 043837 (2014).
- [25] M. H. Schleier-Smith, I. D. Leroux, and V. Vuletić, *Phys. Rev. A* **81**, 021804 (2010).
- [26] Y.-L. Zhang, C.-L. Zou, X.-B. Zou, L. Jiang, and G.-C. Guo, *Phys. Rev. A* **91**, 033625 (2015).
- [27] A. D. Ludlow, M. M. Boyd, J. Ye, E. Peik, and P. O. Schmidt, *Rev. Mod. Phys.* **87**, 637 (2015).
- [28] I. Ushijima, M. Takamoto, M. Das, T. Ohkubo, and H. Katori, *Nature Photonics* **9**, 185 (2015).
- [29] T. Nicholson, S. Campbell, R. Hutson, G. Marti, B. Bloom, R. McNally, W. Zhang, M. Barrett, M. Safronova, G. Strouse, W. Tew, and J. Ye, *Nat Commun* **6**, (2015).
- [30] W. F. McGrew, X. Zhang, R. J. Fasano, S. A. Schäffer, K. Beloy, D. Nicolodi, R. C. Brown, N. Hinkley, G. Milani, M. Schioppa, T. H. Yoon, and A. D. Ludlow, *Nature* **564**, 87 (2018).
- [31] N. D. Lemke, A. D. Ludlow, Z. W. Barber, T. M. Fortier, S. A. Diddams, Y. Jiang, S. R. Jefferts, T. P. Heavner,

- T. E. Parker, and C. W. Oates, Phys. Rev. Lett. **103**, 063001 (2009).
- [32] A. Kawasaki, B. Braverman, Q. Yu, and V. Vuletić, Journal of Physics B: Atomic, Molecular and Optical Physics **48**, 155302 (2015).
- [33] A. Kawasaki, B. Braverman, E. Pedrozo-Peñafiel, C. Shu, S. Colombo, Z. Li, O. Özel, W. Chen, L. Salvi, A. Heinz, D. Levonian, D. Akamatsu, Y. Xiao, and V. Vuletić, Phys. Rev. A **99**, 013437 (2019).
- [34] R. C. Brown, N. B. Phillips, K. Beloy, W. F. McGrew, M. Schioppo, R. J. Fasano, G. Milani, X. Zhang, N. Hinkley, H. Leopardi, T. H. Yoon, D. Nicolodi, T. M. Fortier, and A. D. Ludlow, Phys. Rev. Lett. **119**, 253001 (2017).
- [35] H. Tanji-Suzuki, I. D. Leroux, M. H. Schleier-Smith, M. Cetina, A. T. Grier, J. Simon, and V. Vuletić, in *Advances in Atomic, Molecular, and Optical Physics*, Vol. 60, edited by P. B. E. Arimondo and C. Lin (Academic Press, 2011) pp. 201 – 237.
- [36] M. G. Raizen, R. J. Thompson, R. J. Brecha, H. J. Kimble, and H. J. Carmichael, Phys. Rev. Lett. **63**, 240 (1989).
- [37] P. Münstermann, T. Fischer, P. Maunz, P. W. H. Pinkse, and G. Rempe, Phys. Rev. Lett. **82**, 3791 (1999).
- [38] E. J. Davis, G. Bentsen, L. Homeier, T. Li, and M. H. Schleier-Smith, Phys. Rev. Lett. **122**, 010405 (2019).
- [39] J. Hu, W. Chen, Z. Vendeiro, H. Zhang, and V. Vuletić, Phys. Rev. A **92**, 063816 (2015).
- [40] See supplemental material at xxx link.
- [41] M. Saffman, D. Oblak, J. Appel, and E. S. Polzik, Phys. Rev. A **79**, 023831 (2009).
- [42] B. Braverman, *Cavity Quantum Electrodynamics with Ensembles of Ytterbium-171*, Ph.D. thesis, Massachusetts Institute of Technology (2018).
- [43] B. Braverman, A. Kawasaki, and V. Vuletić, New Journal of Physics **20**, 103019 (2018).
- [44] C. Weedbrook, S. Pirandola, R. García-Patrón, N. J. Cerf, T. C. Ralph, J. H. Shapiro, and S. Lloyd, Rev. Mod. Phys. **84**, 621 (2012).
- [45] T. Opatrny, Phys. Rev. Lett. **119**, 010502 (2017).